10. D. A. Gubaidullin and A. I. Ivandaev, "Characteristic times of phase interaction processes and their effect on dispersion and absorption of acoustic waves in vapor–gas–drop systems," Teplofiz. Vys. Temp., 29, No. 1 (1991).
11. D. A. Gubaidullin and A. I. Ivandaev, "Dynamics of low-amplitude pulse waves in vapor–gas–drop systems," Prikl. Mekh. Tekh. Fiz., No. 2 (1991).
12. V. Sh. Shagapov, "Propagation of small disturbances in a vapor–gas–drop medium," Teplofiz. Vys. Temp., 25, No. 6 (1987).
13. N. A. Gumerov and A. I. Ivandaev, "Sound propagation in polydisperse gas suspensions," Prikl. Mekh. Tekh. Fiz., No. 5 (1988).
14. R. I. Nigmatulin, A. I. Ivandaev, and D. A. Gubaidullin, "The nonmonotonic dependence of sound dissipation on the drop concentration in acoustics of gas suspensions," Dokl. Akad. Nauk SSSR, 316, No. 3 (1991).
15. R. I. Nigmatulin, Dynamics of Multiphase Media [in Russian], Part 1, Nauka, Moscow (1987).
16. N. A. Fuks, Mechanics of Aerosols [in Russian], Izd. Akad. Nauk SSSR, Moscow (1955).

EFFECT OF THE MOTION INSIDE A LIQUID DROP ON ITS RISE IN A VERTICAL TUBE

P. K. Volkov

UDC 532.529.6

1. Introduction. In treating the rise of bubbles in a liquid it is usually assumed that the medium inside the bubble is at rest and the state of the medium can be described by a single constant: the thermodynamic pressure p_g of the gas inside the bubble. For gas or air bubbles rising in a heavy liquid this assumption is justified, since the ratios of the densities and viscosities of the gas and liquid are small and so the medium inside the bubble is light and the friction of the gas against the liquid on the surface of the bubble is small and has a negligible effect on the motion. This assumption is supported by numerous experiments. However for vapor bubbles, such as in Freon, the ratio of the densities is of order 0.1 and the use of the bubble model can lead to inaccurate results.

2. Statement of the Problem and Solution Algorithm. We assume that the medium inside the bubble is a viscous incompressible liquid (a liquid drop moving in a different liquid) with $\rho_1/\rho_2 = 0.1$. We consider hindered motion of the liquid drop in a tube with $\lambda = 0.8$. Here ρ_1 and ρ_2 are the densities of the media inside and outside the liquid drop; $\lambda = a/R_k$, where a is the radius of a sphere whose volume is equal to that of the liquid drop and R_k is the radius of the tube. Since the liquid drop occupies more than half of the tube cross section, the flow of the liquids inside and outside the drop are determined by the nature of the flow through the narrow gap between the wall of the tube and the surface of the drop. For small λ the effect of the tube wall is small, as is shown by calculations of rising bubbles [1], but its effect increases with λ.

The motion inside and outside the liquid drop is described by the Navier–Stokes equations. Consistency conditions must be satisfied on the interface Γ between the two liquids [2]. The velocities and the tangential components of the stress must be equal across the interface, while the normal component of the stress has a jump equal to the magnitude of the capillary pressure. The algorithm for obtaining the numerical solution of the problem is constructed in analogy to [1] and has been described in detail in [3]. The results of a series of calculations are summarized in Fig. 1 in terms of the coordinates $R_\sigma = a/(\nu_2^2/g)^{1/3}$, $R_\nu = a/(\sigma/\rho_2 g)^{1/2}$. A given external medium corresponds to a straight line on the diagram, since $R_\sigma/R_\nu = (g\rho_2^3\nu/\frac{1}{2}\sigma^3)^{1/6} = M^{1/6}$, where M depends only on the physical constants of the external medium (g is the acceleration of gravity, σ is the surface tension on the interface between the media, and ν_1 and ν_2 are the kinematic viscosities of the liquid drop and the external liquid). Because of the large number of dimensionless parameters [3] (we use the Reynolds numbers of the internal and external fluids $Re_1 = u2a/\nu_1$, $Re_2 = u2a/\nu_2$ and the Weber number $We = \rho_2 u^2 2a/\sigma$) it is difficult to generalize the results. Nevertheless the lines of

Novosibirsk. Translated from Prikladnaya Mekhanika i Tekhnicheskaya Fizika, No. 4, pp. 83-94, July-August, 1993. Original article submitted August 13, 1992.

 0021-8944/93/3404-0524$12.50

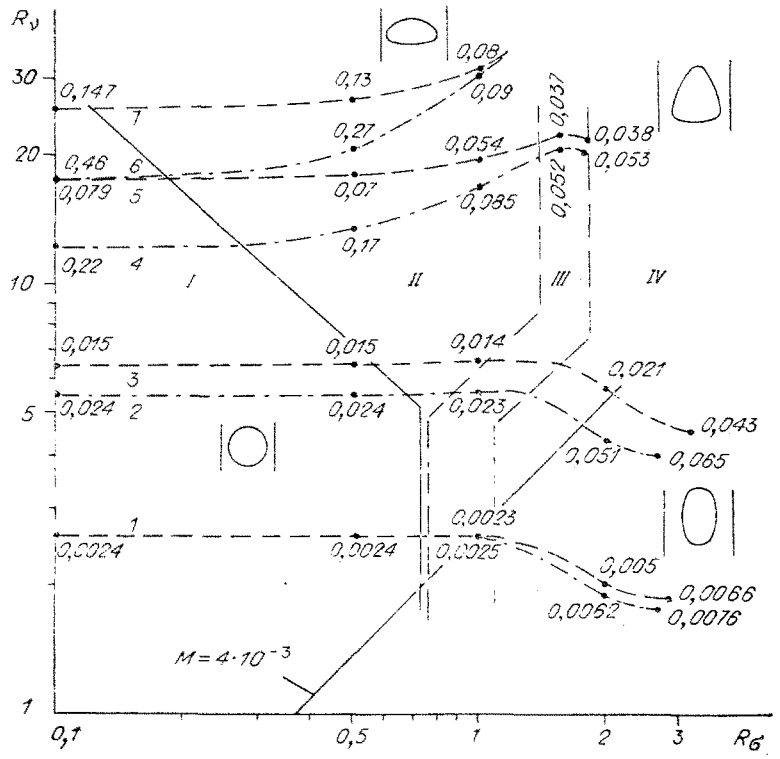

Fig. 1

constant Reynolds number and the Froude numbers ($Fr = u^2/ga$) shown in Fig. 1 provide complete information on the rise velocity u and show the general features of the flow and the effect of the medium inside the drop on its rise. Here curves 1, 3, 5, 7 correspond to $Re_1 = 0.4$ and $Re_2 = 0.4$, 4, 40, 100 and curves 2, 4, 6 correspond to $Re_1 = 60$ and $Re_2 = 4$, 40, 100. For given Re_1, Re_2 calculations were carried out starting from We = 0, where the drop is a sphere. As We increases its shape changes.

3. Rise of Slightly Deformed Drops. Region I in Fig. 1, bounded to the right by the solid slanting line, corresponds to spherical and slightly deformed liquid drops where the ratio of the horizontal to the vertical diameters is less than 1.03. The quantity Fr is practically constant and independent of We for fixed Re_1 and Re_2. Region I was constructed for $Re_1 = 60$ and is practically identical to the analogous region for bubbles [1]. For $Re_1 = 0.4$ the upper slanted part of the boundary of region I rotates to the right by 15-20°.

We first consider the rise of a spherical drop. When $\lambda = 0$ the Navier–Stokes equations can be solved exactly for $Re_2 \ll 1$ (Hill's spherical vortex [4]) and the solution is independent of the medium inside the drop. Here for We = 0 we have a sphere with a = 2 and the boundary condition on the normal component of the stress is satisfied [3]. One would expect that the rise of the liquid drop would continue to be independent of the medium inside for sufficiently small Re_2 and $\lambda > 0$. Calculations with $Re_1 = 0.4$ and 60 for different We practically coincide when Re_2 is small: curve 1 in Fig. 1 corresponds to $Re_2 = 0.4$. There is strong vortex motion inside the drop, as shown in Fig. 2 (the solid lines are the streamlines in a coordinate system fixed to the liquid drop and the dashes represent the velocity vector over the tube cross section). The maximum velocity inside the liquid drop is comparable to the velocity of the liquid through the narrow gap between the wall of the tube and the surface of the drop. At $R_\sigma = 0.1$ we have $M \approx 3 \cdot 10^{-9}$ for curve 1 of Fig. 1, while the value of M for the liquid drop (M_k) varies from 10^{-19} for $Re_1 = 60$ to $3 \cdot 10^{-12}$ for $Re_1 = 0.4$; on the right boundary of region I ($R_\sigma = 0.8$) $M \approx 10^{-3}$ while $M_k = 2 \cdot 10^{-15}$ and 10^{-6}, respectively.

For larger Re_2 the solutions for $Re_1 = 60$ and 0.4 are different (curves 2 and 3 for $Re_2 = 4$ in Fig. 1). However, there are no significant changes in the structure of the flow and the picture is very similar to Fig. 2. At $Re_2 = 40$ the difference between the curves for $Re_1 = 60$ and 0.4 (curves 4 and 5 in Fig. 1) is still greater and changes to the flow structure begin to become noticeable. For example, when $Re_1 = 60$ the lengths of the velocity vectors near the surface of the drop on both sides are longer than in Fig. 2 and when $Re_1 = 0.4$ the rate of rotation of the vortex inside the liquid drop is much smaller (the local

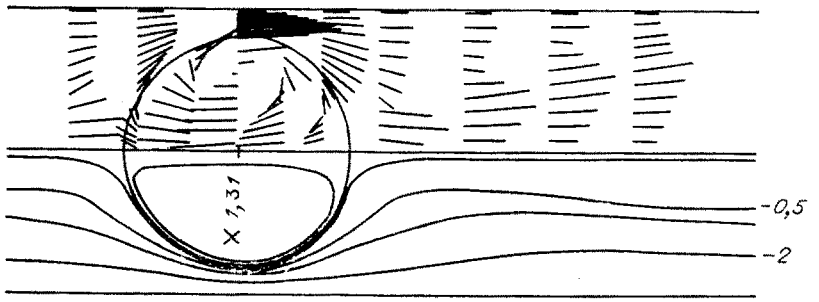

Fig. 2

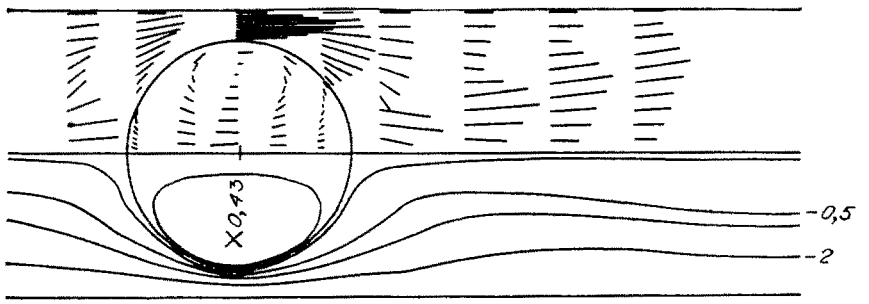

Fig. 3

maximum of the stream function becomes ≈0.4). The maximum velocity inside the liquid drop is now smaller than the rise velocity (Fig. 3, We = 0.0058, R_σ = 0.2, R_ν = 17.5, Fr = 0.074, M = 10^{-13}, M_k = $2\cdot10^{-7}$). The velocity distribution inside the narrow gap is different: the flow of the liquid just outside the surface of the drop is significantly slowed.

Curves 6 and 7 in Fig. 1 correspond to Re_2 = 100. The relationship between the flows for small and large Re_1 is approximately the same as for Re_2 = 40. The flow for Re_1 = 60 is shown in Fig. 4 (We = 0.024, R_σ = 0.17, R_ν = 17.7, Fr = 0.45, M = $1.8\cdot10^{-13}$, M_k = 10^{-15}). At R_σ = 0.1 the values of M for Re_2 = 100, Re_1 = 60 and Re_2 = 40, Re_1 = 0.4 are practically the same. For larger R_σ ($\leq$0.2) there are slight differences in the flow structure and the values of Fr. Therefore, Figs. 3 and 4 illustrate the effect of the medium inside the drop on its rise: M, R_σ, R_ν (and therefore the size of the drop) are approximately the same while M_k differs by more than eight orders of magnitude. The rise velocity of a liquid drop with the smaller value of M_k (Fig. 4) is 2.4 times higher than the rise velocity of a liquid drop of the same volume with the larger value of M_k (Fig. 3). In passing, we point out a simple test of the correctness of the parameter Fr. The square root of the ratio of the Froude numbers (ratio of the rise velocities) should be equal to the ratio of the Reynolds numbers Re_2 of the external liquids if the data correspond to the same point in Fig. 1. In our case the error is <3.6%, which is within the accuracy of determining Fr by equating the frictional force on the surface of the liquid drop to the buoyancy force.

The fact that the data in region I for constant Re_1 and Re_2 are practically independent of R_σ (curves 1-7 are parallel to the R_σ axis) shows that the rise of the drop is determined by the viscous forces and does not depend on the surface tension. The capillary forces are larger than the force of the dynamical interaction and maintain the spherical shape of the drop.

4. Rise of Deformed Liquid Drops in a Tube. As We increases the liquid drop becomes elongated transverse to the direction of rise (region II in Fig. 1). The gap between the surface of the drop and the wall of the tube narrows, which leads to a greater variation in the velocity over the tube cross section. In a viscous medium with sufficiently large M (>10^{-5}) this process is "rapidly stabilized" and the presence of the tube wall begins to be felt, leading to elongation of the front of the liquid drop (region III) and then elongation of its back (region IV). Therefore in region IV the liquid drop is elongated along the tube and the gap between its surface and the solid wall widens. Region III, where the deformation process of the drop changes, is quite narrow and all of the parameters of a problem are significant here. The lines of constant Reynolds number reach local maxima in this region and then decrease monotonically in region IV, again becoming constant for R_σ > 2. The Fr values along these lines decrease with increasing R_σ, reach local minima in region III, and then

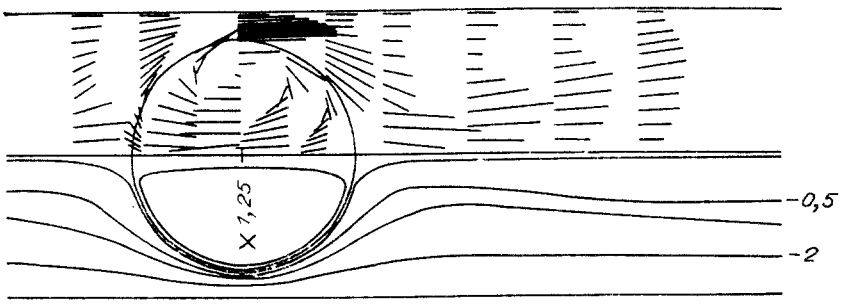

Fig. 4

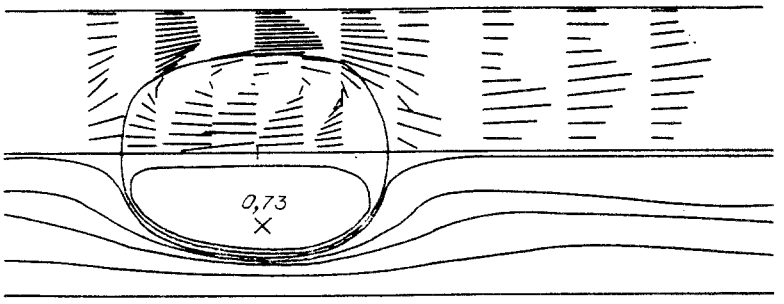

Fig. 5

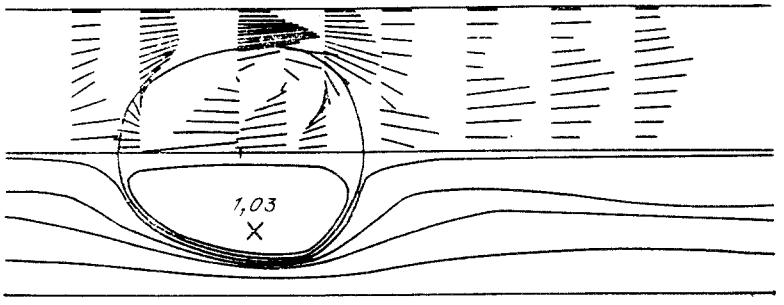

Fig. 6

begin to increase again. Figure 2 (Re_1 = 0.4, Re_2 = 0.4, We = 0.0048, Fr = 0.0023, R_σ = 1, R_ν = 2.58, M = $3.7 \cdot 10^{-3}$, M_k = $3.7 \cdot 10^{-6}$) corresponds to region III. Figure 5 (Re_1 = 0.4, Re_2 = 0.4, We = 0.11, Fr = 0.0066, R_σ = 2.88, R_ν = 1.82, M = 15.8, M_k = 0.016) shows the flow in region IV where the lines of constant Re_1, Re_2 have become horizontal (see Fig. 1). The drop has a prolate shape with a blunt nose (it begins to flatten for $R_\sigma > 2$) and an undulating back. It was not possible to increase R_σ further: the surface of the drop was found to oscillate from iteration to iteration of the calculation. The solutions for different values of We with Re_1 = 60 (Re_2 = 0.4) have the same overall features of the surface deformation, but lie somewhat lower when $R_\sigma > 0.8$ (see Fig. 1). The liquid drop is less elongated than for Re_1 = 0.4 and the motion inside it is more intense. When R_σ = 2.52 a depression appears on the lateral surface of the liquid drop, behind the point of the local maximum of the stream function. For higher R_σ the surface of the drop oscillates from iteration to iteration of the calculation and a steady-state solution is not obtained.

The calculations for Re_2 = 4 with Re_1 = 60 and 0.4 are shown on the diagram of Fig. 1 by the parallel curves 2 and 3. This is the region of the hydrodynamic parameters where the individual features of the media are the same and show up as the geometry of the liquid drop changes (the solutions for curve 3 correspond to liquids with identical dynamical viscosities). The flows for Re_1 = 60, We = 0.05 (Fr = 0.023, R_σ = 1.05, R_ν = 5.6, M = $4.4 \cdot 10^{-5}$, $M_k \sim 10^{-11}$) and Re_1 = 0.4, We = 0.028 (Fr = 0.014, R_σ = 1, R_ν = 6.55, M = $1.2 \cdot 10^{-5}$, M_k = $1.2 \cdot 10^{-4}$) are very similar to Fig. 2 with the motion inside the drop somewhat weaker for Re_1 = 0.4 (the maximum of the stream function is 1.16).

When $R_\sigma \geqslant 2$ the liquid drop is elongated along the tube. Figure 6 corresponds to Re_1 = 60, We = 0.4 (Fr = 0.05, M = 0.01, $M_k \sim 10^{-10}$, R_σ = 1.98, R_ν = 4.28) and Fig. 7 to Re_1 = 0.4, We = 0.18 (Fr = 0.022, M = 0.0023, M_k = 0.023, R_σ = 2.05, R_ν = 5.65). With further increase in We (We = 0.85, R_σ = 2.57, R_ν = 3.95, M = 0.075, M_k = 10^{-9}) the length of the drop for

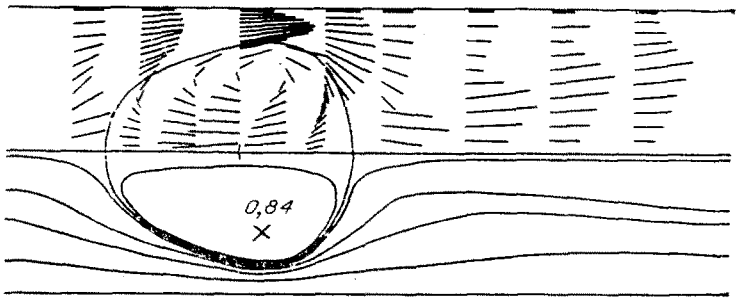

Fig. 7

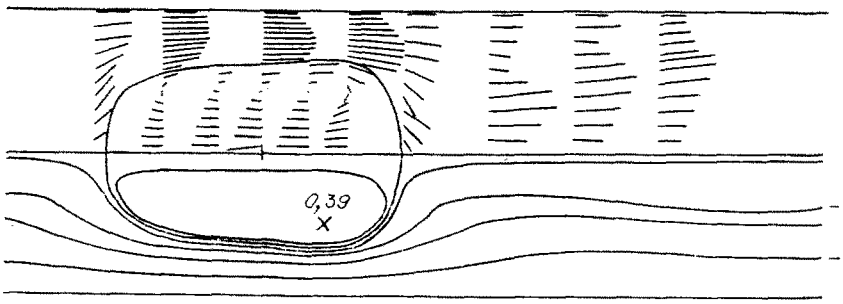

Fig. 8

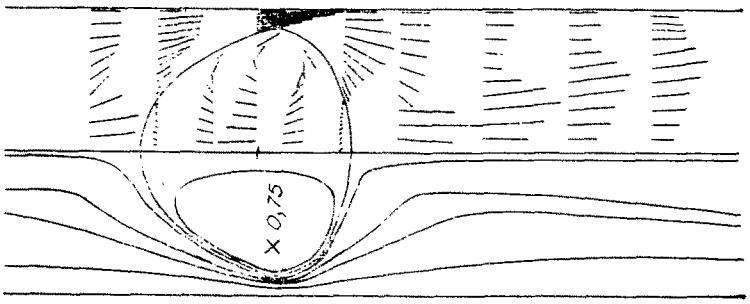

Fig. 9

$Re_1 = 60$ remains the same as in Fig. 6, the undulation at the rear of the drop increases, and the nose is slightly flattened (as in Fig. 5). There are no striking changes in the flow structure. The situation is different for $Re_1 = 0.4$: at $R_\sigma = 2.55$ (We = 0.46, Fr = 0.035, M = 0.022, $M_k = 0.22$) the liquid drop is significantly elongated, but front and rear are little changed. The motion inside the liquid drop decreases and the point of the local maximum of the stream function (equal to 0.53) is shifted back. Figure 8 (We = 0.85, Fr = 0.043, $R_\sigma = 3.15$, $R_\nu = 4.5$, M = 0.11, $M_k = 1.1$) shows the flow corresponding to the horizontal limit of curve 3 (Fig. 1). Part of the lateral surface of the drop is parallel to the tube wall and there is a characteristic broadening of the back of the drop.

In liquids with $M < 10^{-5}$ rising liquid drops are elongated transverse to the tube in a much larger region of We (region II of Fig. 1). The lines of constant Re_1 and Re_2 in the region of spherical bubbles differ more strongly (curves 4, 5 and 6, 7 of Fig. 1), which demonstrates the significant effect of the medium inside the drop on its rise. With increasing We curves 4, 5 and curves 6, 7 begin to converge. The difference between the Fr values on these curves decreases and reaches a minimum in region III, where the deformation process changes and the liquid drop begins to elongate along the axis of the tube. Figure 9 ($Re_1 = 0.4$, $Re_2 = 40$, We = 0.26, Fr = 0.04, $R_\sigma = 1.84$, $R_\nu = 21.7$, $M = 3.6 \cdot 10^{-7}$, $M_k = 3.6 \cdot 10^{-2}$) shows the flow for transition into region IV. The liquid drop becomes wedge-shaped, as in the case of a bubble in this region of R_σ and R_ν (see Fig. 7b of [1]). The liquid inside the drop is practically at rest at the front and rear of the drop and the no-slip condition holds on the outer side of the surface, as in the case of a fixed wall. For large R_σ the surface of the drop changes with time.

The results for $Re_2 = 100$ with $Re_1 = 60$ and 0.4 (curves 6 and 7 in Fig. 1) approach with increasing R_σ. The values of Fr on these curves decrease; they differ by ~12% when $R_\sigma = 1$. Figure 10 shows the flow for $Re_1 = 60$, We = 0.19 (Fr = 0.086, $R_\sigma = 1.04$, $R_\nu = 30.66$, $M = 1.5 \cdot 10^{-9}$, $M_k \sim 10^{-11}$). A strong vortex exists inside the liquid drop and outside it there is a

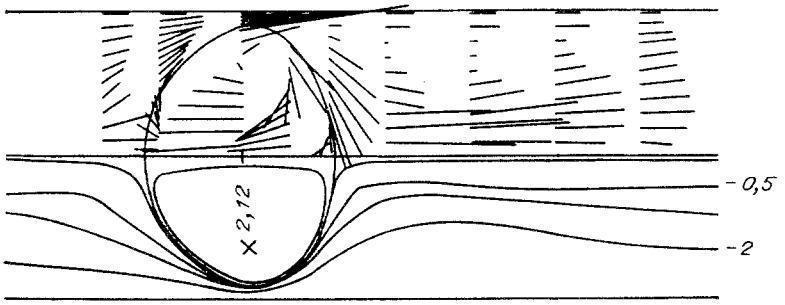

Fig. 10

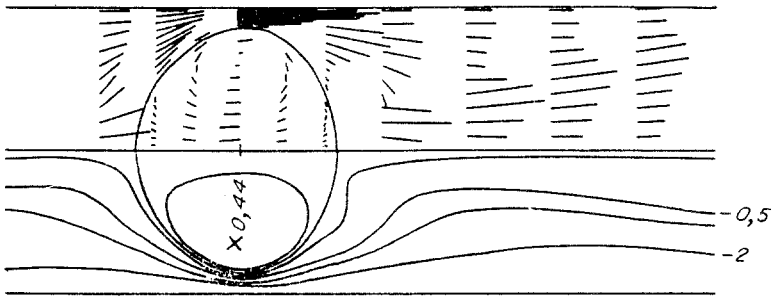

Fig. 11

quiescent zone near the tube wall. Liquid moves along the surface of the drop, flowing around it and creating a jet behind it near the axis. The flow structure strongly recalls the flow near a rising bubble [1]. The form of the flow is quite different for $Re_1 = 0.4$ (Fig. 11, We = 0.17, Fr = 0.066, $R_\sigma = 1.14$, $R_\nu = 33.45$, $M = 1.5 \cdot 10^{-9}$, $M_k = 6 \cdot 10^{-3}$). There is weak vortex motion inside the liquid drop and the streamlines in the external flow breakaway from the back surface of the drop indicating the formation of a quiescent zone behind the drop, which may subsequently lead to flow separation. The results of Figs. 10 and 11 correspond to external liquids with similar values of M. The diameters of the drops differ by less than 10%, while $M_k \sim 10^{-11}$ and $6 \cdot 10^{-3}$. Therefore Figs. 10 and 11 illustrate the effect of the medium inside the drop on its rise in a given external liquid.

5. Friction on the Wall of the Tube and Pressure on the Surface of the Drop. The rise of a liquid drop in a tube with a different quiescent liquid is accompanied by flow of the external liquid downward through the narrow gap between the wall of the tube and the surface of the drop. An important function characterizing the efficiency of the rise is the distribution of friction τ over the wall of the tube. Since $\tau = -2\omega/Re_2$, if we know the vorticity ω on the wall we can determine the losses by integrating this relation over the surface of the tube. The geometrical interpretation of a definite integral is the area under the curve, therefore from a graph of ω we can easily estimate the work done in overcoming the friction of the liquid against the wall and the contribution of different parts of the tube to the work done.

Since the liquid drop rises in a tube with a quiescent external liquid, the friction against the wall is nonzero only at the level of the drop and over a certain distance from it. Graphs of ω are shown in Fig. 12: curves 1-3 correspond to Figs. 2, 5, and 8. Curve 1 corresponds to a slightly deformed sphere. The ω curve is asymmetric about $\theta = \pi/2$. Behind the liquid drop there is a region of positive ω, indicating slowing of the liquid. The positive and negative peaks increase with increasing Re_2. We compare the values of ω in Figs. 3 and 4, which correspond to liquid drops of equal volume rising in the same external liquid. The minimum values of ω are -10 and -7.7. For the dimensional values of ω we have, at the negative peak

$$\frac{\omega_{60}}{\omega_{0,4}} = \sqrt{\frac{Fr_{60}}{Fr_{0,4}}} \frac{\omega'_{60}}{\omega'_{0,4}} = \sqrt{6} \frac{7,7}{10} \simeq 1,9,$$

where the indices on ω and Fr indicate the value of Re_1; the quantity ω' is dimensionless. Since $\tau \sim \rho_2 \nu_2 \omega$, we have $\tau_{60}/\tau_{0,4} \approx 1.9$ and the frictional peak for rise of a liquid drop with $M_k \approx 10^{-15}$ is 1.9 times larger than the peak for a liquid drop with $M_k \approx 10^{-7}$, whereas the rise velocity of the first drop is 2.4 times larger than the second.

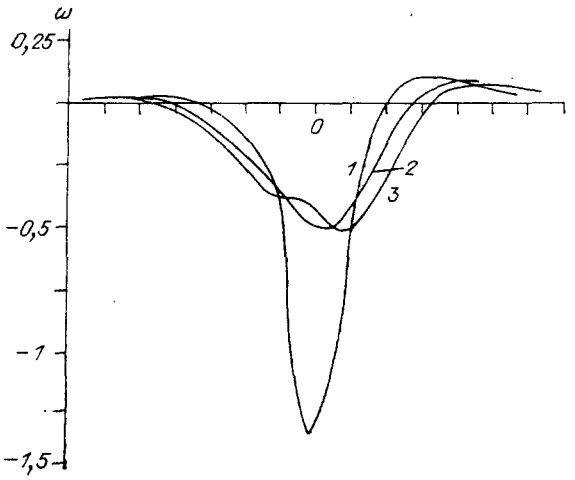

Fig. 12

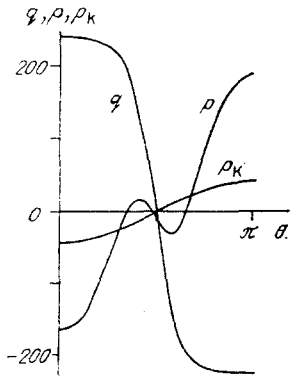

Fig. 13

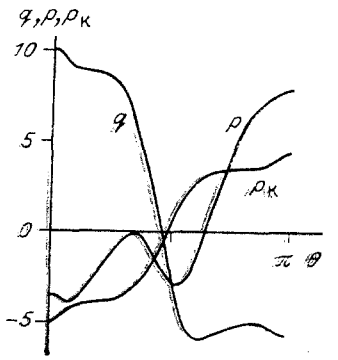

Fig. 14

The analogous relation for Figs. 10 and 11 gives $\omega_{60}/\omega_{0.4} \approx 1.37$ (in this case the graphs of ω are close and the peak values are −30 and −25). Here the rise velocities of the drops are only slightly different.

The total losses for rising drops are composed of two terms: friction of the liquid against the wall of the tube and against the surface of the liquid drop. For large Re_1 the losses on the liquid drop are negligible and the values of Fr and ω on the wall, the shape of the drop, and the flow structure are similar to the case of a bubble. For small Re_1 it can be seen by comparing Fig. 10 with 11 and Fig. 3 with 4 that the no-slip condition holds on the nonmoving (or only slightly moving) part of the boundary. The friction of the liquid against the drop is now significant (flow separation is even possible; see Fig. 11) and the total losses over the flow become large.

The change in the vorticity with increasing deformation of the surface of the liquid drop can be followed by comparing Figs. 2 and 5 and curves 1 and 2 in Fig. 12, which correspond to the same values of Re_1 and Re_2. As the liquid drop elongates along the axis of the tube the gap between it and the tube wall widens and the magnitude of the peak in ω drops. If part of the surface is parallel to the tube wall then a "shelf" appears on the graph of ω. Dips (or bumps) on the surface lead to oscillations in ω (curve 3 of Fig. 12 corresponds to Fig. 8). Therefore small distortions in the shape of the drop (changes in the gap width) are reflected in the vorticity ω and hence in the friction τ over the wall.

An important hydrodynamic characteristic is the pressure p. The problem of the flow of a fluid around a body of given shape can be solved in terms of the variables ψ and ω and the pressure p does not appear explicitly in the solution. It can be found from the solution for ψ and ω by fixing p at a certain point in the region of flow. Usually the so-called generalized pressure q (the algebraic sum of p and the gravitational potential) is determined. This is sufficient, since gravity plays a passive role in the problem. Pressure deviations only show up in comparing the calculated results with the experimental data in a particular liquid and may show up as a shift in p by a constant amount.

In the problem considered here the pressure appears explicitly in the boundary condition on the surface of the liquid drop and is found from the initial equations of motion in a single iteration cycle. The driving force of the rise process is gravity and the quantity Fr, determined by the solution of the problem, appears in the coefficient of this force. Therefore, the pressure is important in the balancing of the active forces (Fr is found by balancing the buoyancy force against the frictional force of the external liquid against the drop) and in maintaining the constant volume of the drop [$Pd = (p_\infty - p_g)2a/\sigma$, where a is given].

Graphs of the pressure over the surface of a spherical liquid drop are shown in Fig. 13 for $Re_1 = 60$, $Re_2 = 0.4$, $We = 0.0001$ ($R_\sigma = 0.16$, $R_\nu = 2.5$). The flow in this case is similar to Fig. 2. Here q and p are the generalized pressure and pressure outside the surface of the drop and p_k is the pressure on the inner side Γ of the drop surface. The Froude number is small, therefore the gravitational potential ($\sim R\cos\theta/Fr$) makes the dominant contribution to q; note that p is nonmonotonic. The velocity gradient is large inside the narrow gap (liquid is accelerated in the converging part and decelerated in the diverging part) and the function p has a local maximum and minimum. The pressure p_k inside the liquid drop corresponds to the

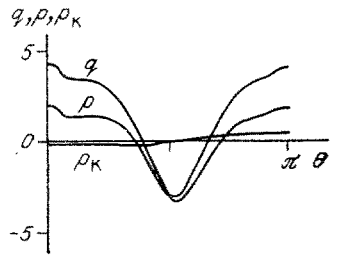

Fig. 15

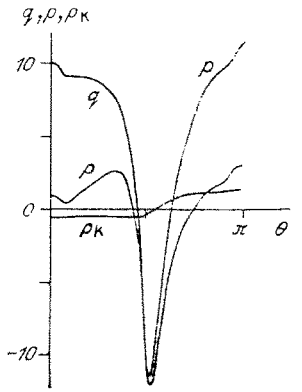

Fig. 16

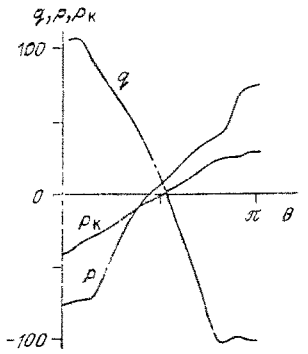

Fig. 17

hydrostatic pressure, even though the flow inside the drop is significant. This is a consequence of the smallness of the parameter ρ_1/ρ_2, which is a coefficient in the dynamical correction to p_k. The pressure graphs for $Re_1 = 0.4$, $Re_2 = 0.4$, $We = 0.0001$ are practically the same as in Fig. 13, except for the initial and final segments of the curves, where the oscillation amplitude is slightly larger.

Figures 14 and 15 correspond to the data of Figs. 3 and 4 for different spherical drops of the same volume rising in the same external liquid. The pressure graphs for the more viscous drop resemble Fig. 13, but p is of order p_k because of the slowing of the external liquid near the drop. Figure 15 corresponds to the case of a bubble: the friction over the surface is small and the pressure increases toward the back. The function p_k is small and practically constant except near $\theta = \pi/2$, where it changes sign.

Deformation of the surface and the narrowing of the gap leads to a redistribution of the pressure and to narrow peaks in the gap region (Fig. 16 corresponds to the data of Fig. 10). These peaks become smoothed out for a more viscous drop. Therefore Figs. 10, 11, and 16 demonstrate the effect of the medium inside the drop on the pressure during its rise.

Elongation of the liquid drop along the axis of the tube leads to changes in the structure of the pressure distribution. The nonmonotonic region of p spreads over the entire lateral surface of the drop and the oscillation amplitude decreases. The function p_k is similar to p. Significant differences exist only near the front of the drop. The pressure graphs shown in Fig. 17 correspond to the data of Fig. 5. The nonmonotonic behavior of p_k and p near the front of the drop occurs because two moving liquids (inside and outside the drop) meet in this region and the spread along the surface, flattening the back of the drop if their dynamical heads are approximately the same.

6. Discussion of the Results. The calculations show that for $Re_1 = 60$ the deformation behavior of the liquid drop and the values of Fr are similar to the case of a bubble [1]. The calculations cover the region of M_k from 10^{-16} ($Re_2 = 100$) with $We = 0.01$ (sphere) to 10^{-11} with $We = 0.19$ (deformed liquid drop) and from 10^{-19} ($Re_2 = 0.4$) with $We = 0.0001$ to 10^{-11} with $We = 0.01$; $M \sim 10^{-14}$ and 10^{-9} for $Re_2 = 100$ and $\sim 10^{-8}$ and 10 for $Re_2 = 0.4$. Solutions for $Re_1 > 60$ in the interval of We (or R_σ) considered here will correspond to liquid drops with still smaller values of M_k. Since ρ_1/ρ_2 is fixed, this implies smaller viscosities and therefore less friction on the surface Γ.

Solutions for $Re_1 = 0.4$ correspond to the rise of more viscous liquid drops with M_k values from 10^{-15} ($Re_2 = 100$) with $We = 0.02$ (sphere) to 0.006 with $We = 0.17$ (deformed drop) and from $\sim 10^{-12}$ ($Re_2 = 0.4$) with $We = 0.00004$ to 0.16 with $We = 0.11$; the parameter M varies from 10^{-16} (spherical drop) for $Re_2 = 100$ to $M = 16$ (elongated torpedo shape) for $Re_2 = 0.4$.

Larger values of M_k than discussed above correspond to solutions with $Re_1 < 0.4$, i.e., more viscous liquid drops (in the limit of a nonmoving liquid) with the velocity of the external liquid equal to zero at the surface of the drop. Solutions corresponding to fixed Re_2 with $Re_1 < 0.4$ lie somewhat higher on Fig. 1 than for $Re_1 = 0.4$. Therefore, by using Fig. 1 and the diagrams of [1] for bubbles the lines of constant Froude number for particular liquid drops can be constructed and the behavior of the rise as a function of the external liquid can be determined. The dimensions of the liquid drops for which solutions can be obtained reach 2-3 times the capillary constant of the external liquid.

In the region of spherical drops and for $Re_2 < 1$ the rise process is independent of the medium inside the drop and the hydrodynamic parameter R_σ: the lines of constant Re_1 and Re_2 and the lines of constant Fr are parallel to the R_σ axis. Two types of behavior are observed in the region of deformed drops. When $Re_2 < 1$ (or for liquids with $M > 10^{-3}$) this "self-similar" behavior breaks down and curve 1 in Fig. 1 bifurcates. For large Re_2 (for liquids with $M < 10^{-6}$) deformation of the drop leads to a reduced sensitivity of the rise velocity to the features of the medium inside the drop: the velocities are close to drops with M_k differing by 5-7 orders of magnitude. Between these two classes of liquids there is an intermediate zone with M from $\sim 10^{-6}$ to 10^{-4}, where the lines of constant Re_1 and Re_2 are practically parallel (curves 2 and 3).

The convergence of curves 4 and 5 on the one hand and 6 and 7 on the other can be explained by the fact that as the drop becomes more deformed the secondary flow has closed streamlines near the wall of the tube behind the drop and at the front of the drop near its surface. The quiescent zones wipe out the features of the flow determined by the medium inside the drop and the rise velocity becomes independent of the liquid inside the drop.

The calculations show that if M_k of the drop is smaller than M of the external liquid then the flow is similar to that near a rising bubble; in the opposite case the motion near the interface between the two media is significantly slowed.

For bubbles rising in a tube it has been shown [5] that in the region where the bubbles become elongated along the axis of the tube the rise is like that of an elongated torpedo ($\lambda = 0.8$), i.e., the rise velocity does not depend on the size. Since the diagrams are qualitatively and quantitatively similar for bubbles and liquid drops, it follows that in region IV of Fig. 1 drops whose equivalent radius is larger than the capillary constant δ_σ rise in hindered conditions as elongated projectiles if $M > 10^{-4}$. In liquids with $M < 10^{-4}$ this regime occurs for drops with radii larger than $2\delta_\sigma$.

The motion of the medium inside the drop does not change the right boundary of region III, where the nature of the deformation changes, from the case of a bubble. The left boundary is shifted so that region III becomes narrower. Hence the motion of the medium inside a bubble leads to a widening of the region of spherical bubbles in liquids with large M. Therefore, in tubes with $R_k < \delta_\sigma$ an increase in the size of the bubble can lead to stoppage because of its "rigidity." The narrowing of region III and the shifting of its upper portion to the right may also explain the stopping of bubbles in capillary tubes for liquids with small M [6]: the bubbles become elongated transverse to the tube and are "blocked."

The value for which the change in the deformation process increases significantly is about an order of magnitude larger for liquids than for bubbles (the slanted part of region III).

In summary, the motion of the medium inside a bubble (small ρ_1/ρ_2) significantly affects its rise velocity in a tube, as well as the flow structure of the liquid near the bubble. Calculations for $\rho_1/\rho_2 = 0.5$ show that the data for constant Re_1 and Re_2 are shifted upward on the (R_σ, R_ν) diagram relative to the data for $\rho_1/\rho_2 = 0.1$ and the same values of Re_1 and Re_2 [3]. The Fr values are smaller and the deformation behavior of the liquid drop remains as before. Therefore the flow regime diagram obtained from the calculations gives a complete picture of the processes accompanying the hindered rise of a liquid drop up to the limit of the "elongated torpedo regime."

LITERATURE CITED

1. P. K. Volkov, "Rise of a gas bubble in a tube filled with a viscous liquid," Prikl. Mekh. Tekh. Fiz., No. 6 (1989).
2. G. K. Batchelor, An introduction to Fluid Dynamics, Cambridge University Press (1973).
3. P. K. Volkov, "Rise of liquid drops in a vertical tube containing a different liquid," in: Simulation in Mechanics [in Russian], Vol. 4(21), No. 5, Computing Center, Inst. of Theoretical and Applied Mechanics, Siberian Branch of the Academy of Sciences of the USSR (1990).
4. M. J. M. Hill, "On a spherical vortex," Phil. Trans. R. Soc. London Ser. A, 185, Part 1 (1984).
5. P. K. Volkov, "Hydrodynamics of bubbles rising in capillary tubes," Sib. Fiz. Tekh. Zh., No. 4 (1991).
6. N. Maeda, "Behavior of a single bubble in quiescent and flowing liquid inside a cylindrical tube," J. Nucl. Sci. Tech., 12, No. 10 (1975).